CHARACTERIZATION OF THE SURFACE PROPERTIES OF TWO PRESSURE SENSITIVE ADHESIVES

By

Hanqi Wen

A thesis submitted to Johns Hopkins University in conformity with the requirements for the degree of Master of Science in Engineering

Baltimore, Maryland

May, 2019

Abstract

Pressure sensitive adhesive (PSAs) are ubiquitous polymers employed as adhesives tapes and sticky notes. PSAs adhere on a substrate after the application of a light pressure and are widely used in many industries such as electronic, medical, or consumer products. In some situations, it is necessary for the PSA make or maintain a bond in a in a humid environment or even underwater. Similarly, PSAs need to adhere to a broad range of surfaces, including skin which can be very compliant. The objective of this work is to understand how the surface and rheological properties of two PSAs are affected by exposure to water as well as to develop model soft substrate to study the effect of substrate compliance on adhesion.

In Chapter 1 the characterization of two PSAs: poly(2-Ethylhexyl acrylate) and poly(2-Ethylhexyl acrylate-co-AA), is presented. The two PSAs are almost identical, except that one of the two contains 5 wt% of acrylic acid as a comonomer. The objective of the work is to understand how the presence of 5 wt% of AA affects the properties of the PSA. We characterize the underwater surface properties of the two PSAs using the contact angle measurements to determine the surface energy and surface pKa. The surface zeta potential to determine the effect of the solution pH on the charge. We then use these

measurements to interpret separate probe-tack adhesion measurements. Our measurements show that the acrylic acid comonomer significantly affects the properties of the PSAs, especially under wet condition where it deprotonates.

In chapter 2, we reports on the synthesis and characterization of the surface and bulk properties of poly(dimethyl siloxane) (PDMS) with different degree of crosslinking. The objective of the work is to study adhesion of PSAs on compliant substrates. To do so, we selected PDMS as a model compliant substrate and report on the change in surface and mechanical properties of PDMS for different degree of crosslinking. Our measurements show a direct relationship between the concentration of crosslinking agent and the elastic modulus (as measured by shear rheology). We also characterized the surface properties of PDMS after an oxygen plasma treatment. We show that stable contact angle measurements are obtained after extraction of unreacted oligomers.

Acknowledgement

Primarily, I would like to pay my authentic thankfulness to Dr. Joelle Frechette who is the tutor and supervisor of my research. To my best appreciate, I am very grateful for her considerable patience in every detail and provided me effect persuasion towards entire research procedure. If there is no help from my supervisor, it was impossible for me to finish my work. Furthermore, her understandings for students and the spiritual encouragements are quite warm when I suffered failures and toughness. It is my honor to have Joelle supervise me on my work.

Here I also want to thank my lovely colleagues who have been encouraging me and supporting me all the time, especially my collaborators, Preetika Karnal and Anushka Jha. Without their trust and help, I couldn't have the strong motivations to urge me working hard on this essay. Thank you all.

Contents

List of Tables

List of Figures

Introduction

Pressure sensitive adhesive (PSA) is a class of polymer that become tacky upon the application of a slight external stress[1]. PSA ubiquitous in many fields such as the electronical industry, medicine industry, and drug delivery[2]. For example, PSAs are used in manufacturing, wound dressing, medical patches that release drug via the skin[3]. Furthermore, PSAs can be easily removed without leaving residues on the substrate surface, for example in tapes and post-it notes.

Generally, the adhesive properties of PSAs are studied in dry environments as they are detached from a rigid substrate. Under these conditions, all the deformation during the detachment occurs in the PSA, and the surrounding environment does not affect the adhesion properties. However, for many practical situations, for example for medical adhesives, the substrate is soft and wet, and the environment is humid or even completely wet with variable pH.
Unfortunately, there are only limited scientific reports addressing how water, and more generally challenging environmental conditions, affects the performance of PSAs[4-6]. For example, consider medical adhesives who need to adhere to skin (compliant) and maintain a bond under water. Adhesion on soft substrates differs

from the adhesion on rigid ones as energy during debonding is also dissipated within the substrate and not only on the adhesive[7].

Here we investigate the properties of two acrylic PSAs. Acrylic-based PSAs are one of the most common class of PSAs, and generally consist of a crosslinked copolymer where the comonomers are selected to control the glass transition temperature (T_g) and the degree of entanglement[8, 9]. We aim to understand how does the PSA underwater surface properties are affected by the pH of bulk, and in turn how do the changes in surface properties influence the PSA adhesion. We also report on preliminary experiments aimed at developing a soft probe that will be employed to study adhesion of PSAs on compliant substrates. Throughout this work, several techniques are employed to investigate the surface change of the PSA in different pH conditions such as contact angle measurements, probe tack measurements, surface energy determination, and surface zeta potential measurement.

Chapter I

Characterization of surface properties of PSA in different pH solution

***Note: Most of the results, writing, and figures have been published in[10] . Most experiments have been performed in collaboration with Preetika Karnal and Anushka Jha.**

1.1 Introduction

This Chapter reports on the characterization of the surface properties of two PSAs in different pH solutions. Surface properties lead to an interfacial bond, for example through van der Waals forces. In addition, for PSAs rate-dependent viscoelastic dissipation in the bulk can amplify, by orders of magnitude, the energy required to detach the adhesive from the substrate. In fact, due to bulk dissipation some PSAs can sustain very large strains (>100%) prior to failure.[7] When PSAs are immersed in water, both the surface and bulk properties could change. For example, water can affect the adhesion of PSAs through different mechanisms. For instance, when surfaces bond together, fluid can remain trapped in the gaps and crevices between surfaces and an additional force might be necessary to squeeze the fluid out, or alternatively fluid can remain trapped sparsely between the surfaces. According to the visible−IR sum-frequency-

generation spectroscopy (SFG), report about the PDMS-sapphire interface points out the existence of trapped water in heterogeneous contact region at the interface. Additionally, Defante et al.[11] found that hydrophobic polymer coatings will rearrange at boundaries which also attribute to trapped water when contact with a hydrophobic PDMS surface in wet conditions. Except for water trapping, chemical adsorption could also play an important role at underwater interface. Zhang et al.[12] reported evidence of chemisorbed interfacial water in the contact region between a fused silica substrate and a film of poly(methyl silsesquioxane). Evidence suggests that water diffused through the interface rather than the bulk, forming hydrogen bonds with the polymer at the surface[13]. Therefore, surface properties such as the wettability and roughness of both surfaces would play an important role in underwater adhesion.

In addition to possible trapped water at in the contact region, the pH of the bulk solution could also influence adhesion. We would expect that the effect of pH would be more pronounced if the PSA contains acid or base groups. The PSAs investigated here are poly(2-Ethylhexyl acrylate) and poly(2-Ethylhexyl acrylate-co-acrylic acid). The latter contains 5-wt%t acrylic acid as a comonomer and is abbreviated as 5% PSA, while former is pure 2-EHA polymer of the same molecular weight, is abbreviated as 0% PSA. The only difference is the presence of acrylic acid, which we would expect causes a pH-responsive adhesion behavior. More importantly, acrylic acid is commonly employed as a comonomer,

therefore it is important to understand how its presence affects underwater adhesion.

1.2 Materials and methods

1.2.1 Material and sample preparation

PSA synthesis

Model pressure sensitive adhesives based on copolymers of 2-ethylhexyl acrylate (2-EHA) and acrylic or homopolymers of 2-ethylhexyl acrylate (2-EHA) were synthesized in a water bath (Launderometer, Atlas) where the polymerization is initiated and occurs at 60°C with continued agitation for 24 hours. After polymerization, bottles are cooled to room temperature and the polymer solutions are used for pressure sensitive adhesives. PSA samples are then analyzed by conventional GPC against polystyrene molecular weight standards using THF as the solvent and eluent. A sample with a composition of 88 mol% of 2-Ethylhexyl acrylate and 12 mol% of Acrylic Acid having a weight average molecular weight (Mw) of 1,200,000 g/mol was selected for the totality of the results showed in this work and a sample of 100 mol% of 2-Ethylhexyl acrylate having a weight average molecular weight (Mw) of 1,200,000 g/mol used as control. Table 1 summarizes detailed GPC characterization of the PSA. An acrylic acid content of 12 mol% (5 wt%) was selected to represent common typical acrylic PSA.

Table 1. Composition and molecular weight result of selected PSAs. Results are averages from duplicate injections. M_n = Number-average molecular weight, M_w = Weight-average molecular weight, M_p = Molecular weight at signal peak, $Đ$ = Dispersity = M_w/M_n (Previously known as polydispersity index)

PSA	*Composition*		*Mn*	*Mw*	*Mp*	*Đ*
	2-EHA (wt%)	*AA (wt%)*	*g/mol*	*g/mol*	*g/mol*	
5%AA	*95*	*5*	*286667*	*1199002*	*1175371*	*4*
0%AA	*100*	*0*	*104000*	*1200000*	*1100000*	*11.6*

The PSA solutions are then coated on a release liner, dried in a convection oven at an average temperature of 150°F, followed by exposure to UV at a set total adsorbed dose of UV-B light = 400 mJ/cm^2 (directly measured using a power puck radiometer) using a processor from Fusion UV-systems for crosslinking, and used as transfer tapes for further evaluation. Dry PSA films of thickness 25 μm are then transferred on PET release liner for adhesion testing. For rheology measurements, stacks of the same material are used.

Buffer solutions preparation

One PBS tablet (Sigma Aldrich) was dissolved in 500mL deionized water to get a PBS solution with 4mM phosphate buffer, 1mM potassium chloride, and 55mM sodium chloride. Deionized water (>18.2 MΩ•cm) was obtained from EMD Milli-Q® Integral Water Purification System. To generate the buffer solution, 10ml of the 4mM stock solution was diluted in 400 ml deionized water to obtain 0.1 mM phosphate buffer solution. NaOH solution (~pH13) and HCl solution (~pH1) were added into this 0.1 mM buffer solution to adjust pH from 3 to 12. The pH of all solutions was monitored with a Mettler Toledo MP220 pH meter. All pH buffer solutions were stored in sealed bag filled with nitrogen and

stored without direct light exposure. pH of the buffer solutions was measured again prior to any measurement.

1.2.2 Contact angle measurements

Contact angles of fluids drop on PSA sample were measured by a goniometer (FTA 125, First Ten Angstroms). A 10 μL sessile droplet is placed on the surface of the PSAs. Advancing and receding contact angles are measured by injecting or retracting fluid from the deposited sessile droplet by syringe pump via a glass capillary needle. The flow rate of fluids is fixed at 20 μL/min. Advancing contact angle is measured first, followed by the receding contact angle. Capillary needle, syringe and plastic tube which is applied to connect needle and syringe are kept in RBS solution for 24 hours and then rinsed with deionized water, dried by nitrogen, rinsed with the probe fluid and filled with the probe fluid. Every data point is repeated at least 3 times and average values are reported along with their standard deviations.

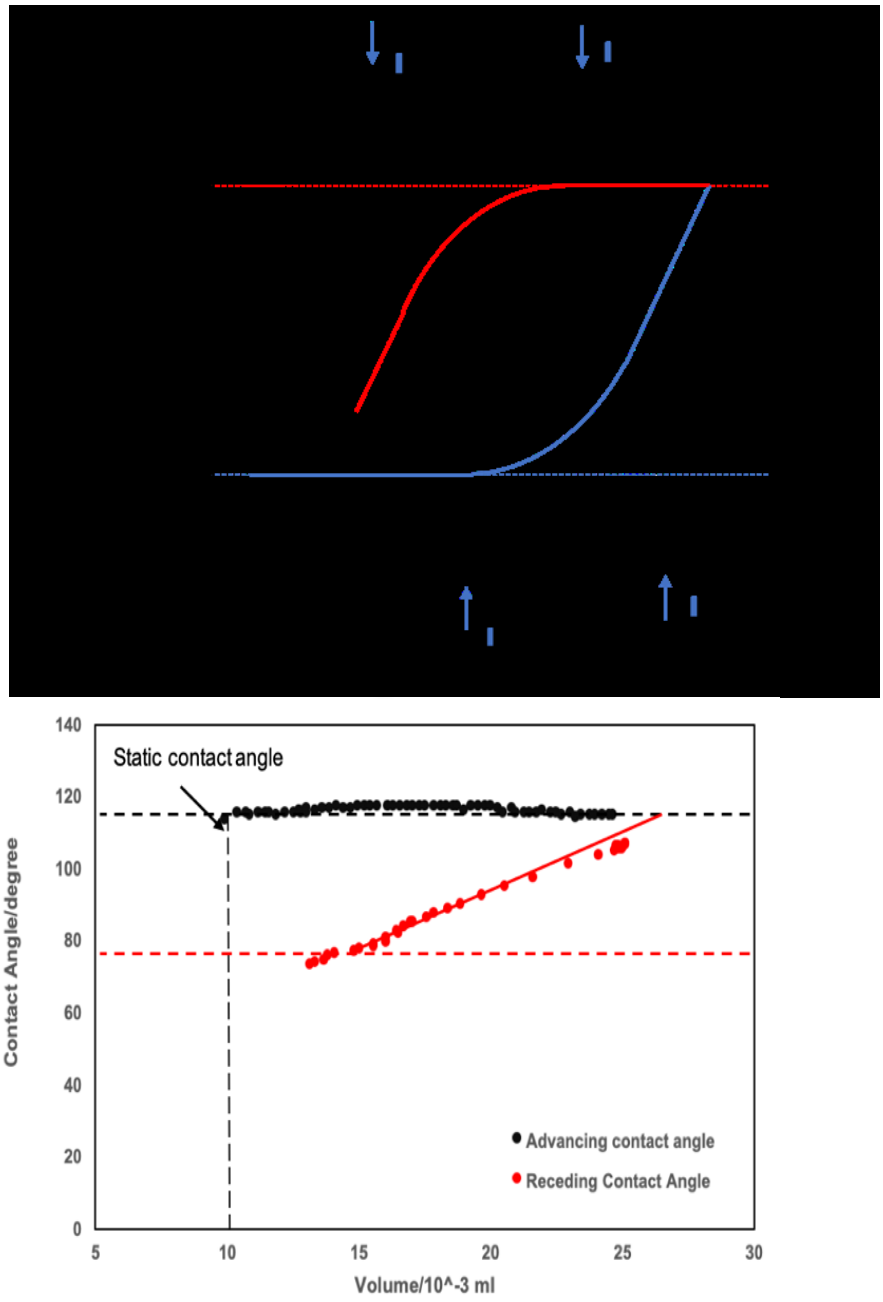

Figure.1 A. (Upper one) Schematic of ideal advancing and receding contact angle measurement. B. (Bottom one) Real experimental result of dynamic contact angle measurement. The Probe liquid used here is pH4 buffer solution. The advancing angle plateau is clear while receding angle is kind of ambiguous.

A theoretical advancing and receding contact angle measurement process is shown in fig.1 A. In fig. 1A, the plateau regions 3 and 5 represent the advancing and receding contact angles, respectively. However, the real experimental result shown in fig. 1B is usually be more complex: the advancing contact angle plateau is easily to recognizable, while receding plateau is typically harder to distinguish. The absence of a clear plateau during the receding contact angle measurements might be due to the adsorption of fluid molecules on the substrate surface. Thus, in this research, advancing contact angle is defined as the corresponding plateau angle in the volume-angle plot while the receding contact angle is defined as the contact angle of the droplet at the moment that the droplet contact line starts to move.

Contact angle hysteresis was also performed on plasma treated PDMS, as discussed in Chapter 2 following the same protocol as described here.

1.2.3 Determination of the surface energy of the PSAs

Calculating surface energy from contact angle measurement is a widely used method developed by Fowkes *et al*[14, 15]. Fowkes' method is based on Young's equation, where an equilibrium multi-phases system (vapor-solid-liquid) is assumed. The contact angle is determined by interfacial tensions:

$$\gamma_3 \cos\theta_{13} = \gamma_1 - \gamma_{13} \tag{1}$$

where γ_1 is the surface energy of PSA in air, γ_3 is the interfacial tension of pH solution in air, γ_{13} is the surface energy of PSA in water and θ_{13} is the contact

angle of pH solution drop on PSA surface in air. The equilibrium film pressure of adsorbed vapor on the solid surface (π_e), is generally small and has been neglected[14]. In equation (number needed), γ_3 and the contact angle θ_{13} is measured from contact angle and pendant drop measurements, while γ_{13} and γ_1 (two unknowns) are not directly measurable from a single contact angle measurement. To solve this problem, Fowkes[15], Owens and Wendt, Girifalco and Good[16] raised different theories succesively based on the same idea of the partition of the surface energy into individual components. Owens' equation is one of the most frequently used:

$$\gamma_1 = \gamma_1^d + \gamma_1^p \tag{2}$$

$$\gamma_{13} = \gamma_1 + \gamma_3 - 2\sqrt{\gamma_1^d \gamma_3^d} - 2\sqrt{\gamma_1^p \gamma_3^p}$$

Combining equation (number needed), we get:

$$\frac{\cos\theta_{13} + 1}{2}\gamma_3 = \sqrt{\gamma_1^d \gamma_3^d} + \sqrt{\gamma_1^p \gamma_3^p} \tag{3}$$

To solve this system of equations with two unknows, two liquids including one polar and one apolar should be chosen to reduce numerical error. Here, I chose water and diiodomethane (Alfa Aesar) as our liquids to measure surface energy of PSA in air. To measure surface energy of PSA in pH solution, I chose pH buffer solution drop (fluid A) and diidomethane (fluid B). The surface tension of the fluids is measured from a pendant drop in air. The reported value[17] of deionized water is 72.8 mJ/m^2. For pH buffer solution, the effect of pH on surface tension is not significant and I obtain 73 ± 1 mJ/m^2, in agreement with literature reports[17]. The measured average surface tension[15] of diiodomethane is 47 ± 1

mJ/m^2 while reported value[18] is 50.8 mJ/m^2. In water, the surface tension of diiodomethane decreased to 39 ± 1 mJ/m^2. Based on Fowkes' method[15], the dispersion and polar surface tension of diiodomethane we used was calculated to be 45 ± 1 mJ/m^2 and 2 ± 1 mJ/m^2, respectively. All following calculation involving the surface tension of diiodomethane uses these measured values.

1.2.4 Probe Tack measurements

Experimental protocol. A custom-built normal and lateral multifunctional force microscope (MFM)[19] is used for probe tack measurements. For the measurements, an OTS coated spherical (plano-convex) lens is mounted on the lens holder attached to the cantilever of the instrument. Fiber optic reflection is used to measure the spring deflection, and is calibrated before each experiment. The PSA films are cut into 15mm x 15mm sized samples. After cutting, the PET release liner is removed, and a sample is placed gently onto a cleaned and dry 46 x 27mm glass slide (Ted Pella). A weighted roller (2kg) is then rolled 20 times onto the sample to remove any trapped air bubbles from the PSA-glass slide interface and apply a high contact pressure. The PSA sample is then mounted on the MFM and held in place by screwing a rectangular holder on top of the PSA-coated glass slide. During a probe tack measurement, the cantilever is lowered at a velocity of 50 μm/s until it applies a 10 mN normal force to the sample, and is held at 10mN using a force feedback loop for a dwell time of 100s. Subsequently the cantilever is retracted at 50 μm/s. Throughout approach, dwell, and debonding images are captured at 70 frames per seconds with an inverted microscope with a 5x objective. The procedure for probe-tack tests in air and in aqueous solutions

are identical, except that for measurements in aqueous solutions the solution is placed on the sample and contained in the MFM bath 10 minutes prior to contact formation. The measurements are performed at room temperature (approximately 23°C) and at less than 50% relative humidity. Each measurement is repeated three times and the reported values represent the average and standard deviation.

Image analysis. Probe tack contact images are processed using ImageJ software (National Institutes of Health, NIH). To process the images during dwell, the out of contact background image is first subtracted from the contact images in aqueous solution, followed by a thresholding and noise reduction steps to improve visualization of the contact area. Subsequently, the images are converted into binary and analyzed through MATLAB to quantify the contact area by calculating the number of black pixels and scaling it by area to number of pixel ratio to find actual image area.

1.2.5 Surface Zeta Potential measurements

PSA samples were cut into small 7 mm x 4 mm strips and attached to the sample holder for the measurement of surface zeta potential (SZP) using Malvern Zetasizer NanoZS surface zeta potential accessory (ZEN1020). Sulfate latex particles of 100nm (Thermo Fisher Scientific) are then dispersed in solutions of different pH. The accessory is immersed in the solutions for SZP measurements. Sulfate latex particles have a stable negative zeta potential of -20 to -50 mV over pH3-pH11. OTS coated glass sheets were cut into small strips of 7mmx4mm and attached to the sample holder using 3M VHB tape for SZP measurements. The

Zetasizer software uses phase analysis light scattering (PALS)[20] to obtain the zeta potential of the tracer particles at different distances from the surface of interest (125, 250, 375 and 500 µm) using the Smoluchowski equation ($U_E = \frac{\varepsilon\zeta}{\eta}$), where the electrophoretic mobility of the particles U_E is converted into the zeta potential ζ of the particle, and ε is the dielectric constant of the fluid while η is the viscosity of the fluid. This method is based on the Doppler effect and dynamic light scattering. In the solution, when the tracer particles whose surface is charged moving under the effect of electronic field generated by the surface (PSAs surface in our case), the incoming light will be scattered by those moving particles. According to the Doppler effect, after scattering, the frequency of outgoing light would change due to particle movement. As a result, frequency shift of incoming and outcoming light is linear to the potential difference between trace and surface[20].

The software then fits the apparent tracer zeta potential as a function of distance to a straight line where the intercept is the apparent zeta potential of the particle very close to the surface. From these measurements, the zeta potential of the surface is obtained from the difference between the zeta potential of the particle far from the surface from the zeta potential of the particles close to the surface ($\zeta_{surface,} = \zeta_{tracer,true} - \zeta_{tracer,apparent}$). Each measurement is repeated thrice and average value is reported along with the standard deviation.

1.3 Results and discussion

1.3.1 Contact angle and surface energy

The advancing and receding water contact angles of the pH buffer solutions on both PSAs are shown in Table 2. The water advancing contact angle on both PSAs is around $\theta_{adv} = 124^o$ at all pH. The receding contact angle on 0% AA is constant across different pH around $\theta_{rec} = 62^o$. A large contact angle hysteresis of $\theta_{adv} - \theta_{rec} \approx 60^o$ is observed for both PSAs. We only observe a pH dependence on the receding contact angle of the 5% PSA samples, where the receding angle decreases from $\theta_{rec} = 62^o$ to $\theta_{rec} = 47^o$ when the pH increases from pH3 to pH11. In the absence of AA groups (0%AA), the surface is not pH responsive and there is no sensitivity of the contact angle to the pH of the probe fluid (advancing and receding). When the contact line of a buffer droplet advances it makes contact with a surface that was initially dry and unaffected by the pH. In contrast, when the contact line recedes it moves on a surface that was in contact with the buffer solution, which can explain why the receding contact angle varies with pH but not the advancing angle. For the receding angle on 5%AA we see a plateau region at 3<pH< 6, and a sharp decrease in the contact angles in the region 6 < pH <12. We suspect that acrylic acid groups on the surface of 5%AA will deprotonate as the pH increases and affect contact angle measurements. Note that the roughness of PSAs sample also plays an important role on the contact angle hysteresis. Even in the absence of carboxyl groups, 0%AA still has a large contact angle hysteresis (that is not pH dependent). Finally, rheology measurements show that the elastic modulus of the PSAs sample is around 10-100 kPa, which means that elastocapillarity effects could alter the contact angle measurements and their interpretation.[21, 22] Fortunately, for

a macroscopic droplet (mm), this phenomenon has a very limited effect on contact angle measurements, even for surfaces as soft as the PSAs investigated here.

Calculating surface energy from contact angle measurement is a widely used method developed by Fowkes, Owens, *et al*[14, 15]. Fowkes' method is based on Young's equation, where an equilibrium multi-phases system (vapor-solid-liquid) is assumed. The contact angle is determined by interfacial tensions:

$$\gamma_3 \cos\theta_{13} = \gamma_1 - \gamma_{13} \tag{4}$$

where γ_1 is the surface energy of PSA in air, γ_3 is the interfacial tension of pH solution in air, γ_{13} is the surface energy of PSA in water and θ_{13} is the contact angle of pH solution drop on PSA surface in air. The equilibrium film pressure of adsorbed vapor on the solid surface (π_e), is generally small and has been neglected[14]. In equation (S8), γ_3 and the contact angle θ_{13} is measured from contact angle and pendant drop measurements, while γ_{13} and γ_1 (two unknowns) are not directly measurable from a single contact angle measurement. To solve this problem, Fowkes[15], Owens and Wendt, Girifalco and Good[16] raised different theories succesively based on the same idea of the partition of the surface energy into individual components. Owens' equation is one of the most frequently used:

$$\gamma_1 = \gamma_1^d + \gamma_1^p \tag{5}$$

$$\gamma_{13} = \gamma_1 + \gamma_3 - 2\sqrt{\gamma_1^d \gamma_3^d} - 2\sqrt{\gamma_1^p \gamma_3^p} \tag{6}$$

Combining equation S8, S9 and S10, we get:

$$\frac{\cos\theta_{13} + 1}{2}\gamma_3 = \sqrt{\gamma_1^d \gamma_3^d} + \sqrt{\gamma_1^p \gamma_3^p} \tag{7}$$

To solve this system of equations with two unknows, two liquids including one polar and one apolar should be chosen to reduce numerical error. Here, we chose water and diiodomethane as our liquids to measure surface energy of PSA in air. To measure surface energy of PSA in pH solution, we chose pH buffer solution drop (fluid A) and diidomethane (fluid B). Based on advancing angles we obtain γ_1=7±2 mJ/m^2 for 5%AA and 8±2 mJ/m^2 for 0%AA, clearly the values are unrealistically low because of surface roughness. The contact angles and surface energy values of both PSAs at different pH are shown in Table 2 and Table 3.

Table 2. Receding (Rec) and advancing (Adv) contact angle (θ) measurements with probe fluid A: pH buffer solution and probe fluid B: diiodomethane on 5%AA and 0%AA.

	pH	Contact angles in degrees			
		Fluid A pH drops		Fluid B Diiodomethane	
		θ_{13}^{Adv}	θ_{13}^{Rec}	θ_{13}^{Adv}	θ_{13}^{Rec}
5%AA	3	125±2	62±5	100±6	30±2
	6	123±1	62±3		
	8	126±1	56±6		
	11	124±1	47±1		
0%AA	3	123±3	64±1	102±5	32±2
	6	124±3	61±2		
	8	124±1	62±2		
	11	123±1	62±1		

Table 3. Surface energy in air and in water calculated from contact angle measurement. 3= water (pH buffer solution), Rec=calculated from receding angle, Adv= calculated from advancing angle, d= dispersion component, p= polar component.

	pH	Surface energy of PSA (mJ/m2)							
		From receding contact angles				From advancing contact angles			
		$\gamma_1^{Rec,d}$	$\gamma_1^{Rec,p}$	γ_1^{Rec}	γ_{13}^{Rec}	$\gamma_1^{Adv,d}$	$\gamma_1^{Adv,p}$	γ_1^{Adv}	γ_{13}^{Adv}
5% AA	3	32	14	47±3	13±3	7	0	7±2	49±2
	6	32	15	47±2	12±2	7	0	7±1	47±1
	8	31	19	50±3	9±3	7	0	7±1	50±1
	11	27	27	54±1	4±1	7	0	7±1	48±1
0% AA	3	32	13	45±2	14±2	8	0	8±1	47±1
	6	32	15	47±1	11±1	8	0	8±2	48±2
	8	32	14	46±1	12±1	8	0	8±2	48±2
	11	30	15	45±1	11±1	8	0	8±1	47±1

1.3.2 Contact angle titration and pKa of carboxyl group on the surface

Based on the pH dependence of the receding angles on 5%AA, we perform a pH titration analysis to calculate the apparent pK_a of the PSA, as shown in Figure 2. I hypothesize that the acrylic acid group is deprotonated at high pH and protonated at lower pH, a difference that is captured by the receding contact angle measurements. This analysis is based on the method from Bain[23]. We consider the PSA surface as a composite surface consisting of surfaces with protonated and deprotonated carboxyl group separately. According to Cassie's law[24], the contact angle of different pH buffer solution on this composite surface is expressed by:

$$\cos\theta_{13} = \alpha_{RCOO^-}\cos\theta_{RCOO^-} + \alpha_{RCOOH}\cos\theta_{RCOOH} \quad (8)$$

where θ_{13} is apparent contact angle of pH buffer solution (3) on 5%AA PSA surface(1), α_{RCOO^-} and α_{RCOOH} are pH dependent area fractions of deprotonated and

protonated PSA surface respectively. θ_{RCOO^-} and θ_{RCOOH} are the contact angles of water on completely deprotonated PSA surface and completely protonated PSA surface respectively θ_{RCOO^-} and θ_{RCOOH} are measured by using extreme high (pH11) or low pH (pH3) solution as drop liquid. Since carboxyl group is distributed uniformly on the PSA surface, the area fractions α_{RCOO^-} and α_{RCOOH} are equivalent to molar fractions of deprotonated and protonated carboxyl group and can be written as:

$$\alpha_{RCOO^-} = \frac{[RCOO^-]}{[RCOO^-]+[RCOOH]}; \alpha_{RCOOH} = \frac{[RCOOH]}{[RCOOH]+[RCOO^-]} \tag{9}$$

Thus, for binary composite surface, obviously we have $\alpha_{RCOO^-}+\alpha_{RCOOH}=1$, where α_{RCOO^-} is also called dissociation ratio and equation S3 becomes:

$$\alpha_{RCOO^-} = \frac{\cos\theta_{13} - \cos\theta_{RCOOH}}{\cos\theta_{RCOO^-} - \cos\theta_{RCOOH}} \tag{10}$$

For monoprotic acid, the definition of dissociation constant K_a is:

$$K_a = \frac{[RCOO^-][H^+]}{[RCOOH]} \tag{11}$$

Combine equation S4 and S6:

$$\alpha_{RCOO^-} = \frac{10^{pH-pK_a}}{1+10^{pH-pK_a}} \tag{12}$$

In S5, since θ_{13}, θ_{RCOO^-} and θ_{RCOOH} are all measurable, the dissociation ratio of carboxyl group in our PSA sample at different pH is easy to be determined. Thus, by plotting pH verses dissociation ratio and performing regression, we can obtain the pK_a of carboxyl group on the surface.

Using this analysis, we obtain an apparent pK_a for 5%AA of 8.7 ± 0.2. We show the titration points and regression curve in Figure 2 and compare them with 0%AA. The pK_a of monomer acrylic acid is 4.25 at room temperature, which is significantly lower than the apparent pK_a of acrylic acid in co-polymerized in p(2-EHA). However, several studies have observed an apparent pK_a ~8 of carboxylic acid SAMs in aqueous solution[25-27]. One possible explanation is that due to dissociation of the surface carboxylic acid groups, the pH at the surface of PSA would be lower than the bulk pH[27]. The real proton concentration near the surface is higher than the bulk and can be approximated as a Boltzmann's distribution, which means that the intrinsic pK_a of the PSA is likely lower than the apparent pK_a. For instance, the pK_a can be estimated as 7.3 using the Nernst equation at an interpolated surface zeta potential of -80mV at pH 8.7. This effect will be detailly discussed later. Additionally, the hydrophobic effect exerted by the adjacent carbon chain group might also contribute to the pKa shift. For example, researchers found that with decrease in composition of carboxylic acid in a mixture of $HS(CH_2)_{10}CO_2H$ and $HS(CH_2)_{10}CH_3$ SAMs on gold from 100% to 14%, the apparent pK_a shifted from pH6 to pH9[28]. In addition, Wasserman *et al.*[29] investigated the acidity of carboxyl groups within a mixture of alkylsiloxane monolayers and showed that the acidity of the carboxyl groups in the monolayer decreased when the fraction of methyl groups increased. This result can be explained by the placement of the acid moiety in an increasingly hydrophobic environment. Urry *et al*.[30] also observed similar effect on protein with aspartic acid group. When the molar fraction of aspartic acid decreases, the fraction of the

protein that is non-polar part increases and the pK_a of aspartic acid shifts from around pH4 to pH6. Urry attributes the pK_a shift to apolar-polar repulsive interaction between aspartic acid and other ammonia acid. With the combined effect of difference in surface and bulk pH and positive shift in pK_a with lower percentage of carboxylic acid groups compared to non-polar groups, the high apparent pK_a of 8.7 for 5%AA PSA is reasonable.

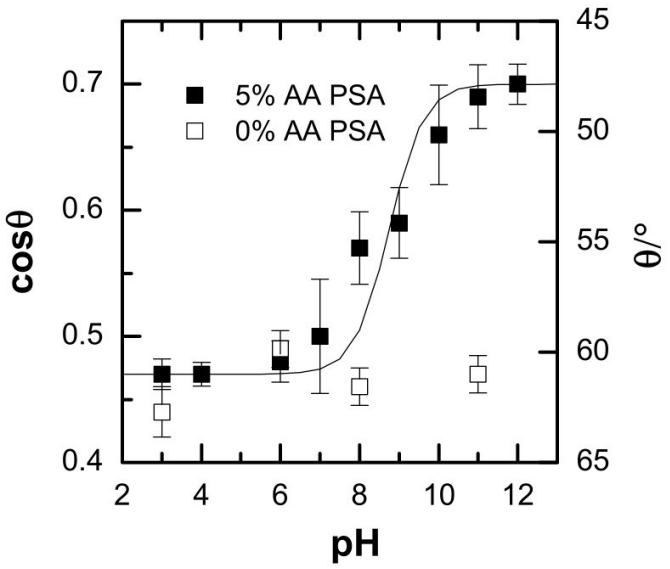

Figure 2. Receding contact angle of pH buffer drops measured on 5% AA PSA (filled) and 0% AA PSA(open). When pH is larger than 6, angle on 5% starts to increase and angle on 0% is approximately constant. Solid line is pH titration curve of receding contact angle on 5% AA PSA. Plateau region is at extreme pH (pH<6 and pH>12) and the increasing region is in the middle region (6<pH<12).

1.3.3 Surface zeta potential and intrinsic pKa

We measured the surface zeta potential (SZP) of the PSAs as well as that of an OTS coated glass slide using dynamic light scattering (Figure 3). The

measurements rely on sulfate latex probe particles, which are stable over the range of pH investigated. We observe that the SZP of 0%AA is nearly constant at -48 mV and shows little to no variation with pH. The SZP of the OTS probe also does not change much with pH, although it shows some variation from –15 ± 6 mV at pH3 to -52 ± 7 mV at pH11. In the absence of carboxylate groups, there is a net negative charge on both the surface of 0%AA and of OTS. Hydroxide ions preferentially adsorb on hydrophobic surfaces (such as OTS and P(2-EHA)) in water leading to a negative surface potential.[31, 32] In contrast to 0%AA and OTS, the SZP of the 5%AA is a strong function of pH, ranging from -1 ± 32 mV at pH3 to -100 ± 7 mV at pH11. Based on these measurements the surface charge density estimated by Grahame equation[33] changes from 0.01 $\mu C/cm^2$ at pH3 to -2.1 $\mu C/cm^2$ at pH11. Likely the SZP becoming more negative with an increase in pH is due to deprotonation of the AA comonomer present on the surface leaving negatively charged COO- groups on the surface. Zimmermann *et al.* reached a similar conclusion when studying polystyrene-polyacrylic acid block co-polymers, and suggested that the pH dependence of the surface charge was due to the dissociation of carboxylic acid groups present on the surface.[34]

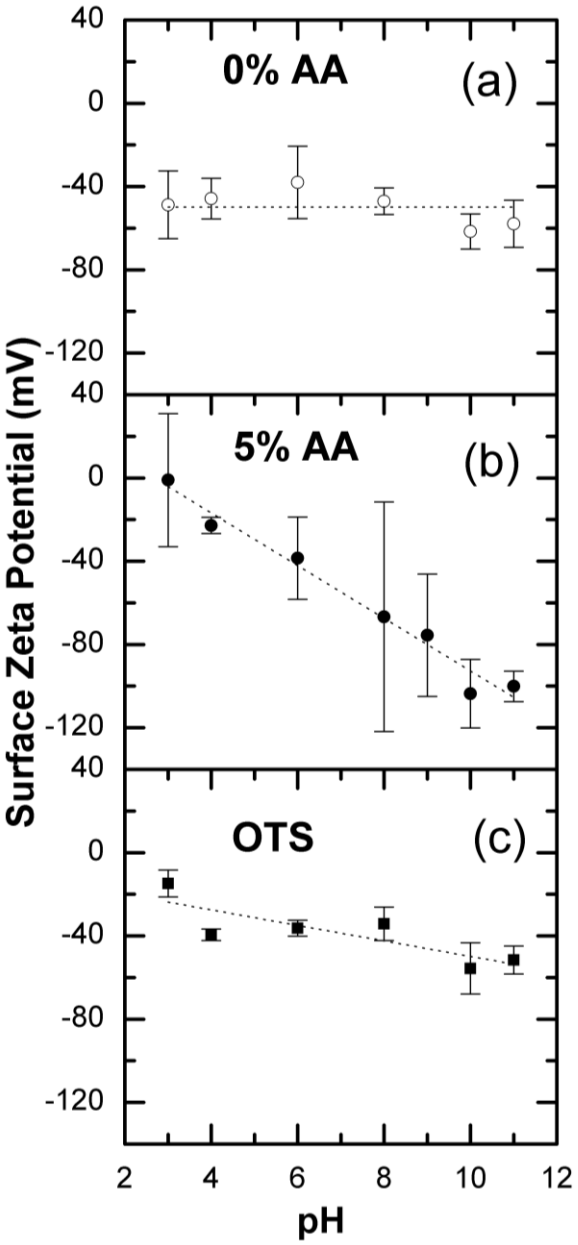

Figure 3. Surface Zeta Potential of (a) 5% AA PSA (b) 0% AA PSA and (c) OTS probe at different pH. Dotted lines are to guide the eye.

With the surface zeta potential result, we can further discuss the charge density on the surface. To simplify the problem, we can assume the buffer

solution only consist of 1:1 electrolytes and then classic Gouy-Chapman model gives the relationship between charge density and potential:

$$\sigma = \sqrt{8\varepsilon\varepsilon_0 kTI}\sinh\left(\frac{e\psi}{2kT}\right) \tag{13}$$

Where σ is surface charge density, I is ionic strength. In addition, dissociation ratio which is the ratio of charged groups and all carboxyl groups is defined as:

$$\alpha = \frac{\sigma}{eN_s} = \frac{[A^-]}{[A^-]+[HA]} = \frac{1}{1+[H^+]_i / K_a} \tag{14}$$

Here the N_S is the total number density of carboxyl group and e is elementary charge. Furthermore, Boltzmann distribution of proton gives:

$$[H^+]_i = [H^+]_b e^{-\frac{e\psi}{kT}} \tag{15}$$

Where the subscribe "b" stands for the concentration in the bulk phase while "i" for the interfacial concentration. Combine equations (13-15), take logarithm to both sides and assume that I (ionic strength) is small enough ($I \to 0$) and SZP is lower than or around -50mV, those equations can be simplified as:

$$\Psi = -\frac{4.606kT}{3e}pH_b + \frac{4.606kT}{3e}\left(pK_a^{int} - \log_{10}\frac{2eN_S}{\sqrt{8\varepsilon\varepsilon_0 RTI}}\right) \tag{17}$$

Assume surface zeta potential approximately equals surface potential:

$$\zeta = -\frac{4.606kT}{3e}pH_b + \frac{4.606kT}{3e}\left(pK_a^{int} - \log_{10}\frac{2eN_S}{\sqrt{8\varepsilon\varepsilon_0 RTI}}\right) \tag{18}$$

From this equation, it's very clear that surface zeta potential is negatively proportional to pH which is consistence to the experimental observation. The slope of experiment is -15mV per unit pH which agrees with equation 18(-17mV per unit pH), too. From fig. 3, when pH~3, the surface zeta potential is around 0. If we plug this into equation 18 and assume that eN_S is around 0.1 to 0.01C/m^2, then we can give a estimation of pK_a as 5, which is very close to free acrylic acid.. This estimation might contains several shortcomings. For example, despite of the deprotonation, the adsorption of ions from the bulk solution to the surface that can also influence the potential-pH curve. Even though the model is not very completed, deprotonation mechanism can still explain lots of experiments observations.

1.3.4 Adhesion of PSA

Data in this section comes from Ref[10]. We performed debonding measurements in aqueous solution of pH3-pH11(Figure 4a,b) for the two PSAs by probe tack. Note that we introduce water prior to contact formation. As shown in Figure 4a, we do not observe a significant effect of the environment (air, pH) on the debonding of the PSA without AA (0%AA).

In contrast, incorporating 5% AA to the PSA leads to debonding forces that are very sensitive to their environment (Figure 4b). First, we see that at pH3, the maximum force of debonding is comparable to that in air. Then, as the pH increases to pH6, pH8 and pH11, the maximum debonding force decreases and is

lower than the one measured in air. In fact, at pH 11 the debonding curve for the two PSAs are nearly identical.

Beyond the peak force, at pH11 0%AA has a broader force curve (detachment occurs over a longer period of time) than 5%AA . While in air the addition of AA as a comonomer leads to a peak debonding force that is 1.4 times larger, at pH 8 and pH 11 the peak forces are still larger but much closer to the one measured for 0%AA. In summary, for underwater and air measurements, the addition of 5 wt% of acrylic acid comonomer to poly-(2EHA) increases the maximum debonding force, except at pH11. For measurements at pH11 the maximum debonding forces for the two PSAs are comparable.

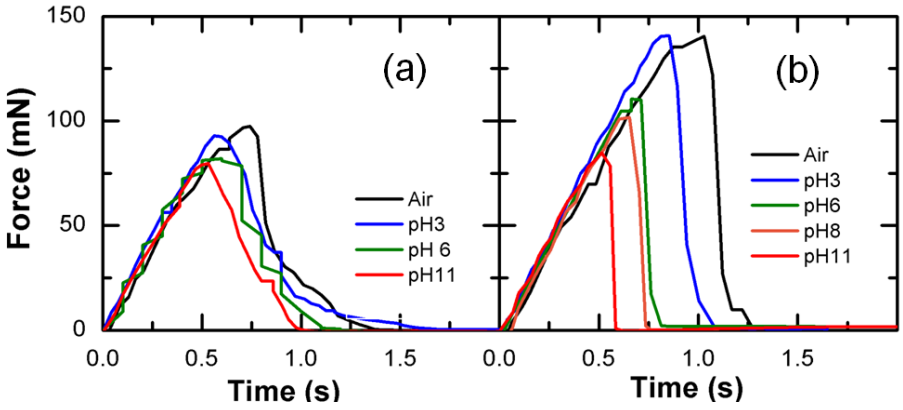

Figure 4. Force curve of a) 0% PSA b) 5% PSA in different circumstance measured by probe tack measurement.

1.4 Conclusion

I investigated the effect of pH of solution on the surface functionalization and characterized deprotonation of the surface by multiple techniques including probe tack, contact angle and surface zeta potential measurement. Contact angle result present a titration curve with pH change. The pKa of acrylic acid is derived

from the titration curve and its bias from the acrylic acid monomer is explained by hydrophobic circumstance and the hydrogen ions distribution. Surface zeta potential of 5% PSA shows approximate linear decreasing with pH increasing. This phenomenon is discussed from the Gouy-Chapman model and several assumptions and the surface energy and surface zeta potential are consistence to each other based on this theory. Probe tack result give an insight into mechanism of adhesion of PSA underwater.

Chapter II

Preparation and characterization of PDMS

2.1 Introduction

PDMS (poly dimethylsiloxane) is a common elastomer employed in medicine, biology research, as well as in soft lithography. PDMS is commercially available and sold as a two-part kit containing two agents, agent A which is the prepolymer of PDMS and agent B that is the cross-linker. PDMS is prepared by mixing those two agents in specific weight ratio and then curing the mixture at a temperature around 350K[35]. Due to its bio-compatibility[36-38], PDMS is widely applied in topologic control of cell fate[39], bioreactor and microchannels[40], biochemical stimuli[41] and immunoassays[42] etc. Apart from biological application, PDMS is also an excellent material in electronic skin study[43] and skin tissue composite[44] mimic. Another key advantage of PDMS is that its surface chemistry can be easily modified by vapor plasma treatment[45] and its bulk rheology property is also tunable by changing stoichiometry of the two components[46]. Because both surface modification and bulk rheology property can significantly influence the performance of PDMS in fields introduced above[47].

In our research, PDMS is used as a soft probe lens to perform probe tack on PSA samples, giving insight into the effect of probe stiffness on the contact

mechanism, experiments mainly conducted by my colleagues Preetika Karnal and Anushka Jha. The Young's modulus or elastic modulus is the simplest metric to characterize stiffness, and for PDMS it's mainly determined by stoichiometry or the weight ratio of agent A agent B (later this stoichiometry ratio is defined as ratio n). The mechanism behind the role of the ratio n in determining the modulus of PDMS is that the cross-linkers connect macromolecules into a three-dimensional polymeric network during the curing process, which is also called cross-linking reaction[46]. Wang et al.[48] measured the elastic modulus by a custom-built compression test apparatus and their result is shown in table 4. Pham et al. [49] used uniaxial tensile testing and shear rheology method to measure elastic modulus of PDMS and their results are in table 5. Considering that PDMS elastic modulus depends on manufacturer and preparing condition (like curing temperature and curing duration), we measured the elastic modulus of all PDMS samples with different n ratio by shear rheology measurement, and later use the PDMS to prepare soft probes.

Table 4. Elastic modulus measured by compression test, Wang et al.

n ratio	E/MPa
5	3.59±0.11
7	2.91±0.036
10	2.61±0.021
16.7	1.21±0.069
25	0.98±0.037
33	0.56±0.021

Table 5. Elastic modulus measured by uniaxial tensile testing and shear rheology, Pham et al.

n ratio	E/kPa
20	400
40	40
50	15
60	5

Except for stiffness, the surface modification and hydrophobicity of PDMS probes are also variables investigated. The as cured PDMS is naturally hydrophobic with a water contact angle of around 110 degree[35, 50, 51]. We performed oxygen plasma treatment on PDMS probes to make the probe surface hydrophilic[52]. Both hydrophobic probe and hydrophilic probe are used to do the probe tack measurements. However, plasma treated PDMS elastomer will gradually lose its hydrophilicity in air[53], making the result less reliable. Thus, the investigation of hydrophobicity recovery of hydrophilic PDMS is necessary. Here, I measured the water contact angle on hydrophilic PDMS which is exposed in air at different time points and the contact angle is the indicator of hydrophilicity.

Apart from surface modification, the presence of unreacted oligomer can also change the surface hydrophilicity and adhesion behavior of PDMS. Choi et al.[54] found that the adhesion energy measured in JKR method of PDMS is different for extracted and unextracted sample. Besides, it is also reported that extracted PDMS is more resistant to hydrophobic recovery or in another words,

more stable in air[55]. Thus, I weighted every sample's weight loss during extraction and calculated the weight loss percentage:

$$\omega = \frac{m_{before} - m_{after}}{m_{before}} \times 100\% \quad (19)$$

By measuring weight loss percentage at different time points, we can monitor the time dependence of extraction effectiveness[56].

As a summary, in this chapter, I characterized 1) chemical stoichiometry relationship with elastic modulus by shear rheology measurement; 2) hydrophilicity of oxygen plasma treated PDMS elastomer; 3) time dependence of hydrophobic recovery in air; 4) time dependence of extraction effectiveness.

2.2 Materials and methods

2.2.1 PDMS preparation and extraction

The PDMS used in this research is purchased from Dow. PDMS elastomer is made by mixing the prepolymer agent (agent A) and the cross-linker agent (agent B). After stirring for at least 5 min, the well-mixed liquid mixture was left in vacuum chamber to remove the bubbles generated from stirring and then poured into mold to fix thickness (around 1.5mm). The de-bubbled mixture was put in oven at constant temperature of 75°C to cure overnight (more than 16 hours). After curing, the sample was cut into 12mm circle using a punch. Then all samples were extracted by hexane for more than 6 hours to remove the extra oligomer or cross-linker. During the extraction process, the PDMS samples can

adsorb large amount of hexane and swells significantly. The extracted samples can increase almost 50% in volume than before extraction. Next step I transferred samples into a mixture of ethanol-hexane to remove the hexane. The samples were first immersed in 1:1 volume ratio mixture (ethanol: hexane) for 5 minutes and then immersed in 2:1, 3:1, 4:1 mixture for 5 minutes for each kind of solvent. Finally, I transferred samples into pure ethanol and sonicated the samples for 15 minutes. The reason for using ethanol-hexane mixture with gradually increased ethanol concentration instead of directly using pure ethanol, is that ethanol can remove hexane rapidly, making PDMS shrink immediately and then the whole polymer would have high risk of breaking. Gradually increase the concentration of ethanol can effectively avoid this problem. The PDMS samples were then dried for more than 12 hours at temperature around 80°C to remove ethanol residue. The weight of PDMS before and after extraction were record.

2.2.2 Rheology measurement

Rheological measurements were performed on PDMS with different ratio n by an AR1500ex rheometer (TA Instruments) with an 8mm diameter parallel plate geometry as the measuring system. The samples were trimmed into 8mm circle and around 1.5mm in thickness before measurement. A strain amplitude of 1% was used in frequency sweep experiments (1-100 rad/s) to obtain the storage (G') and loss (G'') shear moduli of the PDMS sample and the normal force is kept as constant around 10N. The duration of each measurement was ~3 minutes. All the measurements were carried out at 22.4 °C. Each measurement is repeated three times and the reported values represent the average and standard deviation.

2.2.3 Oxygen plasma treatment and hydrophobicity recovery

Hydrophilic PDMS elastomer are functionalized by plasma treatment. Samples are exposed to O_2 plasma for 5 s at 50 W in a homemade induction plasma reactor at 300 mTorr. Once functionalization ended, the water contact angle on one piece of PDMS was immediately measured and I started to timing. Other samples in same plasma treatment round were stored and naturally exposed to air. When the time goes to 5mins, 10mins, 30mins, 1hour, 4hour, 1 day, 3days, and 4days, water contact angle of samples with corresponding exposure duration were measured. The ratio n of PDMS used in hydrophobicity recovery experiment is 10.

2.3 Results and discussion

2.3.1 Time dependence of extraction

The weight change over time of n10, n30 and n40 PDMS sample was monitored and the results are shown in table 5 and the weight loss percentage is plotted versus time in figure 5. For all samples, longer extraction time gives higher weight loss percentage but for n10, the this effect is quite limited while for n30 and n40 long time extraction can significantly improve the effectiveness.

The weight loss actually is the extra PDMS oligomer that didn't crosslink to the network. For Sylgard 184, 10:1 is designed as stoichiometry balance thus n10 has very low extracted weight loss, which is also supported by reported

value[56]. n10 reaches extraction equilibrium around 2h and 4h for n30 but for n40, we need longer extraction (more than 6h) to determine suitable extraction time.

The comparison between large and small n40 sample told us that small samples get higher extraction efficiency than larger one. The mechanism for extraction is diffusion and for large dimension, free oligomer take longer time to diffuse to surface. Thus, for larger sample, longer extraction time is necessary.

Table. 6 Extraction effectiveness of n10, n30 and n40 PDMS samples. m_{before} is the weight before extraction; m_{after} is the weight after extraction; $\omega = \frac{m_{before} - m_{after}}{m_{before}} \times 100\%$ means the weight loss percentage. n10 and n30 samples were measured from 1h to 5h with interval of 1h; n40 is from 2h to 6h with interval of 2h. 2 sets of n40 samples (large size and small size) were analyzed here to figure out the size effect.

Extraction Duration/h		1	2	3	4	5	6
n10	m_{before}/mg	149.6	155.5	166.7	140.0	158.1	
	m_{after}/mg	144.7	149.4	160.2	134.1	151.3	
	ω/%	3.3	3.9	3.9	4.2	4.3	
n30	m_{before}/mg	348.7	329.9	346.2	342.7	364.4	
	m_{after}/mg	306.9	282.8	295.3	288.7	306.7	
	ω/%	12.0	14.3	14.7	15.8	15.8	
n40 (Small)	m_{before}/mg		258.4		164.5		278.8
	m_{after}/mg		199.7		121.8		199.1
	ω/%		22.7		26.0		28.6
n40 (Large)	m_{before}/mg		965.1		1026.5		840.6
	m_{after}/mg		817.9		840.1		656.7
	ω/%		15.3		18.2		21.9

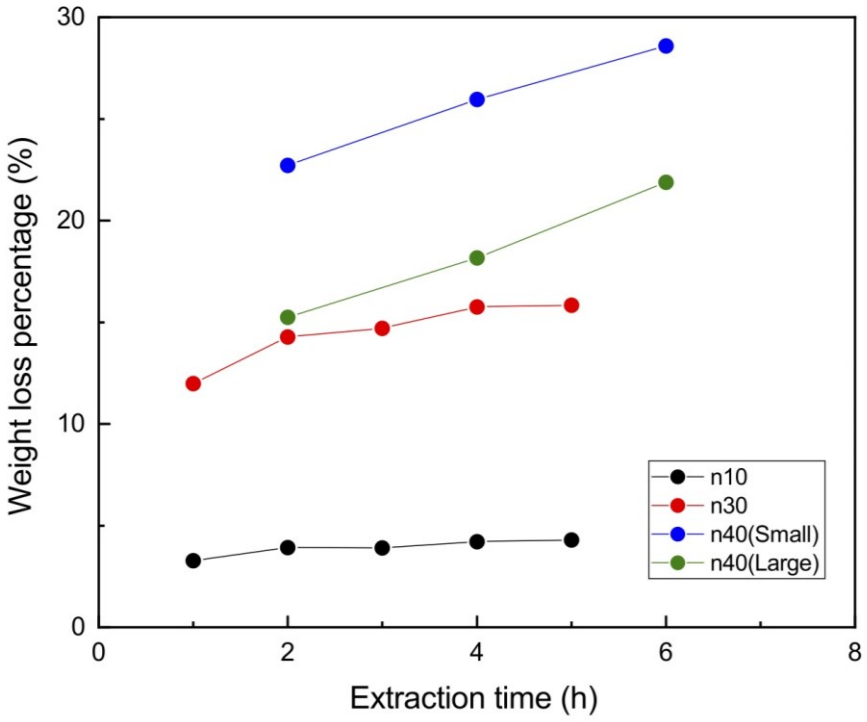

Figure 5. Weight loss percentage at different extraction duration for n10, n30, n40 PDMS sample.

2.3.2 Rheology and elastic modulus of PDMS

Storage shear modulus, loss shear modulus and the ratio of those two modulus (tanδ) are plotted versus angular velocity of the rotating plate (fig.5) and this result agrees with expectations. First, with increasing *n* or decreasing of the concentration of cross-linker, both storage shear modulus and loss shear modulus decreases while tanδ increases. tanδ represents a measure of damping in the material. In another words, higher tan δ indicates the viscoelastic material has a higher viscous components in the complex modulus. From the view of energy, higher tanδ also means during the process of deforming and recovering, the

material would dissipate more energy than those material with lower tanδ. Second, when the n is larger than 25 or 30, shear modulus of PDMS will not continue to decrease. For n30, n45 and n50, their modulus curves overlap with each other because their curing reaction completed imperfectly. When the concentration of cross linker is too low for the PDMS to form, extra PDMS monomer cannot form a polymer architecture and they are removed during the extraction step. That means that the real prepolymer/crosslinker ratio in PDMS for n30, n45 and n50 is not the *n* number obtained from the initial stoichiometry. This observation is also supported by the extraction weight loss. Weight loss percentage is larger for increasing *n*, for $n<30$, this ratio is around 10% to 15% while for $n>30$ sample, this number goes to 25% and even more, which means more monomer is wasted.

Compared to shear modulus, elastic modulus or Young's modulus is more commonly used to represent the stiffness of solid sample. Even though PDMS is not a perfect elastic material and its dynamic modulus is function of shear rate and angular velocity, the elastic modulus calculated from the method for ideal elastic material can still give the relative stiffness of PDMS with different *n*. Classic theory suggests that the material's shear modulus (G), elastic modulus (E) and Poisson ratio (ν) follows the equation:

$$E = 2G(1+\nu) \tag{19}$$

And the shear moduli of viscoelastic material is the modulus of complex shear moduli:

$$|G| = |G^*| = \sqrt{(G')^2 + (G'')^2} \tag{20}$$

For PDMS, its Poisson ratio is very close to 0.5 (0.4995) so the Young's modulus for PDMS with different *n* is estimated as:

$$E = 3\sqrt{(G')^2 + (G'')^2} \tag{21}$$

Results is shown in fig.6. As the discussion above, the Young's modulus dramatically decreases with increasing of *n* and stop at 30. For n>30 sample, they have similar young's modulus.

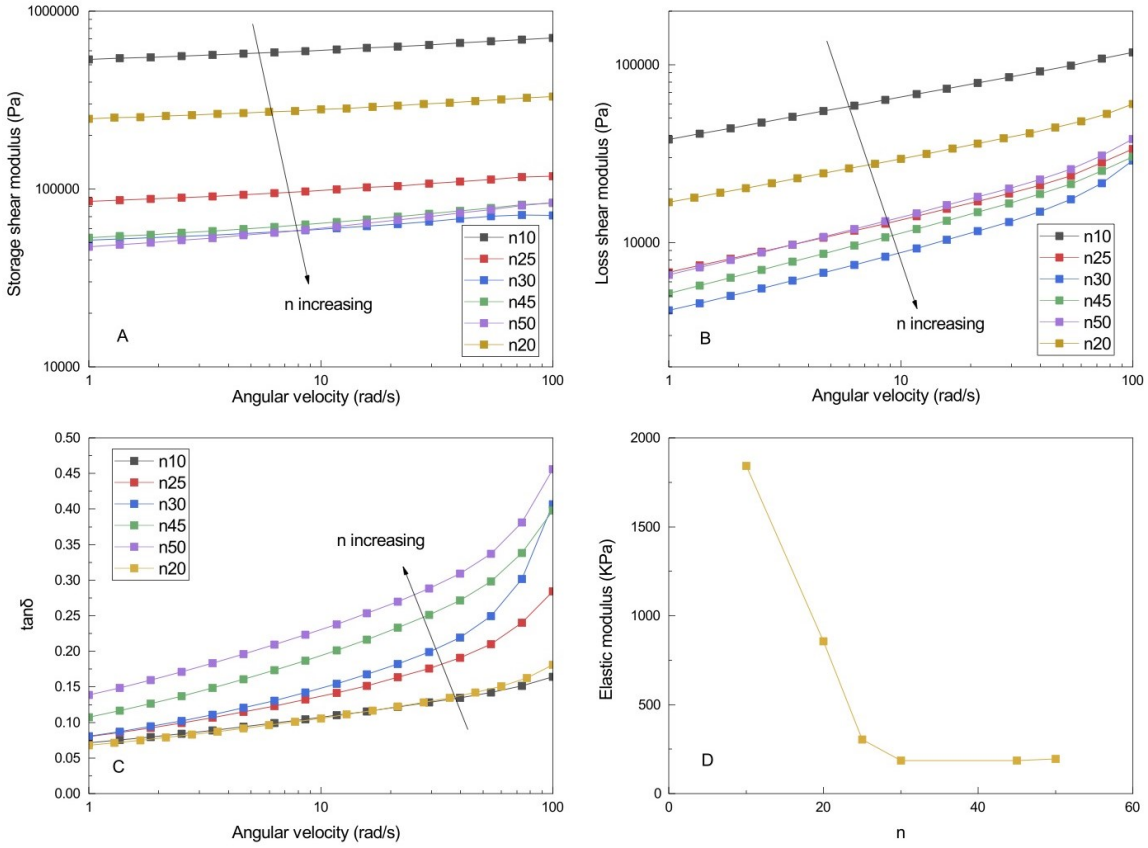

Figure.6 Rheology properties A. Storage modulus B. loss modulus and C. tanδ of different PDMS versus the angular velocity; D. elastic modulus versus ratio n.

2.3.3 Hydrophobicity recovery

The hydrophobicity recovery results are also consistent with expectations. The longer exposure time will lead to the higher water contact angle or in another words, higher hydrophobicity. When the PDMS sample is just taken out of the plasma chamber, the contact angle is low, around 10 degrees. It's necessary to mention that the contact angle measurement by Goniometers has high uncertainty when the contact angle is below 20 degrees. Generally, if the contact angle is smaller than 20 degrees, then the liquid is considered perfectly wetting for the given solid. Thus, we can draw the conclusion that hydrophilic PDMS lose its hydrophilicity after exposure for 30mins; between 1 hour and 4hours, the hydrophobicity of PDMS dramatically increases; after 3 days, the PDMS almost goes to initial hydrophobic state with water contact angle around 100 degree.

Table 7. Water contact angle on oxygen plasma treated PDMS that exposed to air for different duration

Exposure duration	Water contact angle/ degree
~0mins	~10
5 mins	14.74
10 mins	16.16
30 mins	23.03
1 hours	27.34
4 hours	71.36
1 day	78.52
3 days	98.01
4 days	99.54

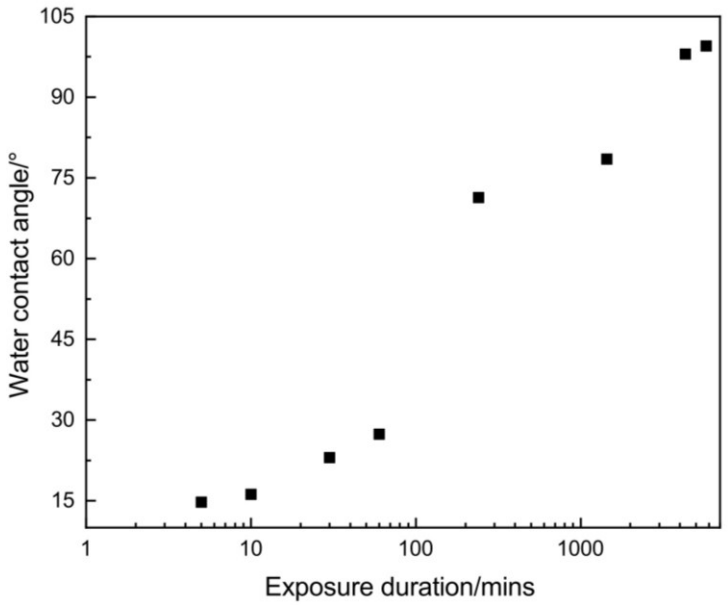

Figure 7. Water contact angle on plasma treated PDMS time dependence curve. After oxygen plasma treatment, PDMS surface is hydrophilic functionalized but due to exposure to air, hydrophobicity would increase with exposure time.

To ensure the reliability of probe tack measurement, after plasma treatment, the hydrophilic PDMS probe should be used in half hour or the surface energy of probe would change and additionally give a less accurate result of probe tack.

2.4 Conclusions

To further dig into the soft probe contact, the bulk rheological measurements of the PDMS is performed. The relationship between cross linker concentration (n value) and the complex shear modulus is clarified. I also raised a new protocol for the soft PDMS purification to prevent the PDMS sample from breaking during the traditional extraction process. The surface hydrophobicity recovery is investigated to figure out how long that plasma treated PDMS can maintain hydrophilicity.

Bibliography

1. Czech, Z.; Kowalczyk, A.; Kabatc, J.; Świderska, J., Photoreactive UV-crosslinkable solvent-free acrylic pressure-sensitive adhesives containing copolymerizable photoinitiators based on benzophenones. *European Polymer Journal* **2012,** *48* (8), 1446-1454.
2. Pizzi, A.; Mittal, K. L., *Handbook of adhesive technology, revised and expanded*. CRC press: 2003.
3. Wang, T.; Lei, C. H.; Dalton, A. B.; Creton, C.; Lin, Y.; Fernando, K. S.; Sun, Y. P.; Manea, M.; Asua, J. M.; Keddie, J. L., Waterborne, nanocomposite pressure-sensitive adhesives with high tack energy, optical transparency, and electrical conductivity. *Advanced Materials* **2006,** *18* (20), 2730-2734.
4. Wang, T.; Canetta, E.; Weerakkody, T. G.; Keddie, J. L., pH dependence of the properties of waterborne pressure-sensitive adhesives containing acrylic acid. *ACS APPL MATER INTER* **2009,** *1* (3), 631-639.
5. Gurney, R. S.; Morse, A.; Siband, E.; Dupin, D.; Armes, S. P.; Keddie, J. L., Mechanical properties of a waterborne pressure-sensitive adhesive with a percolating poly (acrylic acid)-based diblock copolymer network: Effect of pH. *Journal of colloid and interface science* **2015,** *448*, 8-16.
6. Lakrout, H.; Sergot, P.; Creton, C., Direct observation of cavitation and fibrillation in a probe tack experiment on model acrylic pressure-sensitive-adhesives. *The Journal of Adhesion* **1999,** *69* (3-4), 307-359.
7. Creton, C., Pressure-sensitive adhesives: an introductory course. *MRS Bulletin* **2011,** *28* (06), 434-439.
8. Lindner, A.; Lestriez, B.; Mariot, S.; Creton, C.; Maevis, T.; Lühmann, B.; Brummer, R., Adhesive and rheological properties of lightly crosslinked model acrylic networks. *The Journal of Adhesion* **2006,** *82* (3), 267-310.
9. Creton, C.; Ciccotti, M., Fracture and adhesion of soft materials: a review. *Reports on Progress in Physics* **2016,** *79* (4), 046601.
10. Karnal, P.; Roberts, P.; Gryska, S.; King, C.; Barrios, C.; Frechette, J., Importance of substrate functionality on the adhesion and debonding of a pressure sensitive adhesive under water. *ACS Applied Materials & Interfaces* **2017**, 42344–42353.
11. Defante, A. P.; Burai, T. N.; Becker, M. L.; Dhinojwala, A., Consequences of water between two hydrophobic surfaces on adhesion and wetting. *Langmuir* **2015,** *31* (8), 2398-2406.

12. Zhang, X.; Myers, J. N.; Bielefeld, J. D.; Lin, Q.; Chen, Z., In situ observation of water behavior at the surface and buried interface of a low-k dielectric film. *ACS applied materials & interfaces* **2014,** *6* (21), 18951-18961.
13. Luo, M.-C.; Zeng, J.; Fu, X.; Huang, G.; Wu, J., Toughening diene elastomers by strong hydrogen bond interactions. *Polymer* **2016,** *106*, 21-28.
14. Owens, D. K.; Wendt, R., Estimation of the surface free energy of polymers. *Journal of applied polymer science* **1969,** *13* (8), 1741-1747.
15. Fowkes, F. M., Attractive forces at interfaces. *Industrial & Engineering Chemistry* **1964,** *56* (12), 40-52.
16. Girifalco, L.; Good, R. J., A theory for the estimation of surface and interfacial energies. I. Derivation and application to interfacial tension. *J. Phys. Chem. A.* **1957,** *61* (7), 904-909.
17. Beattie, J. K.; Djerdjev, A. M.; Gray-Weale, A.; Kallay, N.; Lützenkirchen, J.; Preočanin, T.; Selmani, A., pH and the surface tension of water. *Journal of Colloid and Interface Science* **2014,** *422*, 54-57.
18. Van Oss, C. J.; Giese, R. F.; Li, Z.; Murphy, K.; Norris, J.; Chaudhury, M. K.; Good, R. J., Determination of contact angles and pore sizes of porous media by column and thin layer wicking. *Journal of Adhesion Science and Technology* **1992,** *6* (4), 413-428.
19. Roberts, P.; Pilkington, G. A.; Wang, Y.; Frechette, J., A multifunctional force microscope for soft matter with in situ imaging. *Review of Scientific Instruments* **2018,** *89* (4), 043902.
20. Corbett, J. C.; McNeil-Watson, F.; Jack, R. O.; Howarth, M., Measuring surface zeta potential using phase analysis light scattering in a simple dip cell arrangement. *Colloids and Surfaces A: Physicochemical and Engineering Aspects* **2012,** *396*, 169-176.
21. Roman, B.; Bico, J., Elasto-capillarity: deforming an elastic structure with a liquid droplet. *Journal of Physics: Condensed Matter* **2010,** *22* (49), 493101.
22. Style, R. W.; Jagota, A.; Hui, C. Y.; Dufresne, E. R., Elastocapillarity: Surface tension and the mechanics of soft solids. *Annual Review of Condensed Matter Physics* **2017,** *8* (1), 99-118.
23. Colin, D. B.; Whitesides, G. M., A study by contact angle of the acid-base behavior of monolayers containing. omega.-mercaptocarboxylic acids adsorbed on gold: an example of reactive spreading. *Langmuir* **1989,** *5*, 1370-1378.
24. Cassie, A., Contact angles. *Faraday Discuss* **1948,** *3*, 11-16.
25. Hu, K.; Bard, A. J., Use of atomic force microscopy for the study of surface acid− base properties of carboxylic acid-terminated self-assembled monolayers. *Langmuir* **1997,** *13* (19), 5114-5119.
26. Godínez, L. A.; Castro, R.; Kaifer, A. E., Adsorption of viologen-based polyelectrolytes on carboxylate-terminated self-assembled monolayers. *Langmuir* **1996,** *12* (21), 5087-5092.
27. Fears, K. P.; Creager, S. E.; Latour, R. A., Determination of the surface pK of carboxylic-and amine-terminated alkanethiols using surface plasmon resonance spectroscopy. *Langmuir* **2008,** *24* (3), 837-843.

28. Bain, C. D.; Whitesides, G. M., A study by contact angle of the acid-base behavior of monolayers containing. omega.-mercaptocarboxylic acids adsorbed on gold: an example of reactive spreading. *Langmuir* **1989,** *5* (6), 1370-1378.
29. Wasserman, S. R.; Tao, Y. T.; Whitesides, G. M., Structure and reactivity of alkylsiloxane monolayers formed by reaction of alkyltrichlorosilanes on silicon substrates. *Langmuir* **1989,** *5* (4), 1074-1087.
30. Urry, D.; Gowda, D.; Peng, S.; Parker, T.; Harris, R., Design at nanometric dimensions to enhance hydrophobicity-induced pKa shifts. *Journal of the American Chemical Society* **1992,** *114* (22), 8716-8717.
31. Beattie, J. K., The intrinsic charge on hydrophobic microfluidic substrates. *Lab on a Chip* **2006,** *6* (11), 1409-1411.
32. Zimmermann, R.; Dukhin, S.; Werner, C., Electrokinetic measurements reveal interfacial charge at polymer films caused by simple electrolyte ions. *The Journal of Physical Chemistry B* **2001,** *105* (36), 8544-8549.
33. Israelachvili, J. N., *Intermolecular and surface forces*. Academic press: 2011.
34. Zimmermann, R.; Norde, W.; Cohen Stuart, M. A.; Werner, C., Electrokinetic characterization of poly (acrylic acid) and poly (ethylene oxide) brushes in aqueous electrolyte solutions. *Langmuir* **2005,** *21* (11), 5108-5114.
35. Feng, J.-T.; Zhao, Y.-P., Influence of different amount of Au on the wetting behavior of PDMS membrane. *Biomedical Microdevices* **2008,** *10* (1), 65-72.
36. El-Ali, J.; Sorger, P. K.; Jensen, K. F. J. N., Cells on chips. **2006,** *442* (7101), 403.
37. McDonald, J. C.; Whitesides, G. M. J. A. o. c. r., Poly (dimethylsiloxane) as a material for fabricating microfluidic devices. **2002,** *35* (7), 491-499.
38. Bélanger, M. C.; Marois, Y. J. J. o. B. M. R. A. O. J. o. T. S. f. B., The Japanese Society for Biomaterials,; Biomaterials, T. A. S. f.; Biomaterials, t. K. S. f., Hemocompatibility, biocompatibility, inflammatory and in vivo studies of primary reference materials low‐density polyethylene and polydimethylsiloxane: A review. **2001,** *58* (5), 467-477.
39. Chen, C. S.; Mrksich, M.; Huang, S.; Whitesides, G. M.; Ingber, D. E. J. S., Geometric control of cell life and death. **1997,** *276* (5317), 1425-1428.
40. Hung, P. J.; Lee, P. J.; Sabounchi, P.; Lin, R.; Lee, L. P., Continuous perfusion microfluidic cell culture array for high-throughput cell-based assays. **2005,** *89* (1), 1-8.
41. Takayama, S.; Ostuni, E.; LeDuc, P.; Naruse, K.; Ingber, D. E.; Whitesides, G. M., Subcellular positioning of small molecules. *Nature* **2001,** *411* (6841), 1016-1016.
42. Sato, K.; Yamanaka, M.; Takahashi, H.; Tokeshi, M.; Kimura, H.; Kitamori, T., Microchip-based immunoassay system with branching multichannels for simultaneous determination of interferon-γ. **2002,** *23* (5), 734-739.
43. Ho, D. H.; Sun, Q.; Kim, S. Y.; Han, J. T.; Kim, D. H.; Cho, J. H. J. A. M., Stretchable and multimodal all graphene electronic skin. **2016,** *28* (13), 2601-2608.
44. Lee, W.; Debasitis, J. C.; Lee, V. K.; Lee, J.-H.; Fischer, K.; Edminster, K.; Park, J.-K.; Yoo, S.-S. J. B., Multi-layered culture of human skin fibroblasts and keratinocytes through three-dimensional freeform fabrication. **2009,** *30* (8), 1587-1595.

45. Jin Ho, L.; Jong Woo, P.; Hai Bang, L., Cell adhesion and growth on polymer surfaces with hydroxyl groups prepared by water vapour plasma treatment. *Biomaterials* **1991,** *12* (5), 443-448.
46. Chambon, F.; Winter, H. H. J. J. o. R., Linear viscoelasticity at the gel point of a crosslinking PDMS with imbalanced stoichiometry. **1987,** *31* (8), 683-697.
47. Park, J. Y.; Yoo, S. J.; Lee, E.-J.; Lee, D. H.; Kim, J. Y.; Lee, S.-H. J. B. J., Increased poly (dimethylsiloxane) stiffness improves viability and morphology of mouse fibroblast cells. **2010,** *4* (3), 230-236.
48. Wang, Z.; Volinsky, A. A.; Gallant, N. D., Crosslinking effect on polydimethylsiloxane elastic modulus measured by custom-built compression instrument. **2014,** *131* (22).
49. Pham, J. T.; Schellenberger, F.; Kappl, M.; Butt, H.-J., From elasticity to capillarity in soft materials indentation. *Physical Review Materials* **2017,** *1* (1), 015602.
50. He, B.; Lee, J.; Patankar, N. A., Contact angle hysteresis on rough hydrophobic surfaces. *Colloids and Surfaces A: Physicochemical and Engineering Aspects* **2004,** *248* (1), 101-104.
51. Bongaerts, J. H. H.; Fourtouni, K.; Stokes, J. R., Soft-tribology: Lubrication in a compliant PDMS–PDMS contact. *Tribology International* **2007,** *40* (10), 1531-1542.
52. Bodas, D.; Khan-Malek, C., Formation of more stable hydrophilic surfaces of PDMS by plasma and chemical treatments. *Microelectronic Engineering* **2006,** *83* (4), 1277-1279.
53. Fritz, J. L.; Owen, M. J. J. T. J. o. a., Hydrophobic recovery of plasma-treated polydimethylsiloxane. **1995,** *54* (1-4), 33-45.
54. Choi, G. Y.; Kim, S.; Ulman, A., Adhesion Hysteresis Studies of Extracted Poly(dimethylsiloxane) Using Contact Mechanics. *Langmuir* **1997,** *13* (23), 6333-6338.
55. Zhou, J.; Ellis, A. V.; Voelcker, N. H., Recent developments in PDMS surface modification for microfluidic devices. *ELECTROPHORESIS* **2010,** *31* (1), 2-16.
56. Esteves, A. C. C.; Brokken-Zijp, J.; Laven, J.; Huinink, H. P.; Reuvers, N. J. W.; Van, M. P.; de With, G., Influence of cross-linker concentration on the cross-linking of PDMS and the network structures formed. *Polymer* **2009,** *50* (16), 3955-3966.

Biographical Statement

Hanqi Wen is a MSE student at the John Hopkins University, Whiting School of Engineering. He works at Dr. Frechette Lab in Department of Chemical Engineering and Biomolecular Engineering. He received a bachelor's degree in chemical engineering from Tsinghua University. He is interested in interfacial science, adhesion phenomenon and pressure sensitive adhesives.